Taylor & Francis
Taylor & Francis Group

Journal of Macromolecular Science, Part A
Pure and Applied Chemistry

ISSN: 1060-1325 (Print) 1520-5738 (Online) Journal homepage: https://www.tandfonline.com/loi/lmsa20

Kinetic modeling of vinyl acetate telomerization catalyzed by metal transition complexes under thermal and microwave heating

Porfirio López-Domínguez, Jessica Olvera-Mancilla, Joaquín Palacios-Alquisira, Larissa Alexandrova, Marc A. Dubé & Eduardo Vivaldo-Lima

To cite this article: Porfirio López-Domínguez, Jessica Olvera-Mancilla, Joaquín Palacios-Alquisira, Larissa Alexandrova, Marc A. Dubé & Eduardo Vivaldo-Lima (2018) Kinetic modeling of vinyl acetate telomerization catalyzed by metal transition complexes under thermal and microwave heating, Journal of Macromolecular Science, Part A, 55:3, 231-242, DOI: 10.1080/10601325.2018.1424549

To link to this article: https://doi.org/10.1080/10601325.2018.1424549

Published online: 17 Jan 2018.

JOURNAL OF MACROMOLECULAR SCIENCE, PART A: PURE AND APPLIED CHEMISTRY
2018, VOL. 55, NO. 3, 231–242
https://doi.org/10.1080/10601325.2018.1424549

Kinetic modeling of vinyl acetate telomerization catalyzed by metal transition complexes under thermal and microwave heating

Porfirio López-Domínguez[a], Jessica Olvera-Mancilla[b], Joaquín Palacios-Alquisira[b], Larissa Alexandrova[c], Marc A. Dubé[d] and Eduardo Vivaldo-Lima[a]

[a]Facultad de Química, Departamento de Ingeniería Química, Universidad Nacional Autónoma de México, Ciudad de México, México; [b]Facultad de Química, Departamento de Fisicoquímica, Universidad Nacional Autónoma de México, Ciudad de México, México; [c]Instituto de Investigaciones en Materiales, Universidad Nacional Autónoma de México, Ciudad de México, México; [d]Department of Chemical and Biological Engineering, Centre for Catalysis Research and Innovation, University of Ottawa, 161 Louis Pasteur Pvt., Ottawa, Ontario, K1N 6N5, Canada

ABSTRACT

A kinetic model for the redox-initiated radical telomerization of vinyl acetate activated by microwave irradiation is presented. Four approaches based on the "microwave" or "thermal" effects were used to study the cases under microwave irradiation. One of the models assumes microwave-induced generation of radicals from monomer. The second model considers higher reaction temperatures than those reported in the experiments. The third model assumes that microwave radiation affects specifically catalyst-involved reactions. The fourth model is a combination of the second and third ones. The kinetic model captures well the effect of initiator, catalyst and solvent contents, as well as absence or presence of microwave irradiation, on polymerization rate and molecular weight development. Limiting monomer conversions and fairly constant values of number average molecular weight and molar mass dispersity were predicted by the model, which agrees with experimental observations.

ARTICLE HISTORY
Received February 2017
Revised November 2017
Accepted January 2018

KEYWORDS
microwave irradiation; telomerization; vinyl acetate polymerization; kinetic modeling; ATRP catalysts

1. Introduction

Microwave-assisted synthesis (MAS) relies on the application of microwave irradiation (MI) as the energy source driving chemical reactions. Polar reagents are adequate for MAS since they are good microwave-absorbing materials, compared to non-polar ones.[1–2] Some of the main advantages of MAS include: volumetric heating, selective heating of strongly microwave-absorbing reagents in heterogeneous mixtures and superheating of solvents at normal pressure.[3] The advantages of MAS have favored the production of (bio)polymer materials by step-growth, chain-growth, ring-opening and metathesis polymerizations.[4–9]

The use of MI as a heating source in reversible deactivation radical polymerization (RDRP, also known as controlled radical polymerization, CRP) is of particular interest. Well-defined and low dispersity polymers can be obtained by using RDRP.[10–16] However, a drawback of RDRP is that increasing the degree of livingness implies lowering polymerization rate. The usefulness of MI in RDRP has been proven in atom transfer radical polymerization (ATRP),[17–21] nitroxide-mediated radical polymerization (NMRP),[22] and reversible addition-fragmentation radical polymerization (RAFT).[23–25] The obtained experimental results in such cases show that: (i) higher polymerization rates under MI conditions, compared to conventional heating (CH), are indeed possible; (ii) controlled growth during polymerization, thus obtaining low dispersity polymers, was observed; and (iii) the polymerizations were claimed to proceed under isothermal conditions, as monitored by an infrared sensor (IRS). In contrast, only slight to moderate improvement in either RDRP[16–29] or conventional free radical polymerization (FRP)[30] under MI conditions has been observed in some cases. It has been suggested that the spectacular rates of polymerization observed in microwave ovens are caused by superheating of the reaction mixture. This is likely due to underestimation of the actual internal temperature by IRS. In order to make fair comparisons, accurate measurement of temperature within the microwave oven is necessary. Polymerization studies carried out using both IRS and optic fiber probes (OF) have shown the importance of employing appropriate temperature monitoring devices.[31,32]

There is a debate in the literature on the effect of MI on polymerization kinetics; namely, if there is a true "microwave effect" (ME, a chemical modification of the reaction mechanism or a specific reaction with an unusually high kinetic rate constant), or if the actual effect is only thermal (TE, non-constant temperature profiles in the reaction mixture caused by MI).[26–30]

The modeling of free radical polymerizations under MI includes approaches based on ME or TE. One of the approaches considering ME is the microwave-induced generation of free radicals from monomer, which has been implemented in modeling studies of emulsion polymerization,[33–34] NMRP,[35] ATRP,[36] and RAFT.[37,38] Zetterlund et al.[38] used three approaches, one based on TE and two

CONTACT Eduardo Vivaldo-Lima vivaldo@unam.mx Universidad Nacional Autonoma de Mexico, Ingenieria Quimica, Mexico City 04510, Mexico.

on ME, to study the kinetics of the microwave-assisted RAFT polymerization of styrene (Sty) with cyanoisopropyl dithiobenzoate and AIBN. In their first approach, the polymerization was assumed to proceed at higher reaction temperatures than those recorded experimentally (TE). In the second approach, higher reaction rates for the propagation and addition steps were considered (ME). Finally, in their third approach, they assumed that free radicals from monomer were produced from MI (ME). The second approach agreed better with their experimental data. The propagation and addition kinetic rate constants under MI were one order of magnitude higher than those under CH.[38] On the other hand, step temperature profiles have been considered in the MI ATRP of Sty and MMA, where there is a sudden change in the rate of polymerization.[36]

In the case of MI RAFT polymerization of vinyl acetate (VAc), using ethylxanthogenacetic acid (EXGA) as a RAFT agent, Roy et al.[39] observed that the rate of polymerization was seven times faster in the case of MI, compared to CH, while the measured molecular weights matched the theoretical values in both cases.

Recently, Olvera-Mancilla et al.[40] studied the Ru(II) catalyzed polymerization of vinyl acetate in the presence of ATRP initiators, under CH and MI. They evaluated the performance of four Ru(II) catalysts. Low conversions were attained in all cases. The highest conversions were obtained with CCl_4, which acted as both initiator and chain transfer agent, leading to non-controlled polymerization and therefore, to the formation of telomers.

In this contribution, we study the kinetic behavior of the redox-initiated radical (RIR-) telomerization of vinyl acetate under CH and MI using modeling tools. The effect of MI was captured by using three different modeling approaches, two based on ME and one on TE.

2. Experimental

Most of the experimental data used to test our models were reported in Olvera-Mancilla et al.[40] However, a few extra experiments on RIR-telomerization of VAc under CH were carried out for completeness and assessment of experimental error.

2.1. Materials

Reagent $RuCl_3.nH_2O$ was purchased from Strem and used without any purification. Vinyl acetate monomer (VAc, > 99%, Aldrich) was passed through a neutral alumina column, distilled under reduced pressure, and stored under nitrogen. Sodium hidroxide (NaOH, 97%), potassium hexafluorophosphate (KPF_6, 99%), acetonitrile (MeCN, HPLC grade, 99.9%), dichloromethane (CH_2Cl_2, HPLC grade, 99.9%), *N,N*-dimethylbenzylamine ligand (C_6H_4-2-CH_2NMe_2, 99%), aluminum isopropoxide (Al(O*i*-Pr)$_3$, 99.9%), anhydrous anisole (99%), dimethyl sulfoxide (DMSO, HPLC grade, 99%), *N,N*'-dimethylformamide (DMF, HPLC grade, 99.9%), tetrahydrofuran (THF, HPLC grade, 99.9%), and carbon tetrachloride initiator (CCl_4, 99.9%) were purchased from Aldrich and used as received.

2.2. General procedure for synthesis of ruthenium complexes

Complex $[Ru(\eta^6\text{-}C_6H_6)(C_6H_4\text{-}2\text{-}CH_2NMe_2)(MeCN)]PF_6$ (**1**) was prepared as reported in the literature.[41,42]

2.3. Polymerization of vinyl acetate under conventional heating

VAc polymerizations were carried out in solution (anisole/VAc; 30/70 v/v), under nitrogen atmosphere, in sealed glass tubes. A typical reaction using an initial molar ratio of [M]/[YZ]/[C] = 200/1/1 proceeded as follows: ruthenium complex **1** (C, 100 mg, 0.2 mmol) was added to a 25 mL Schlenk flask and degassed by vacuum/nitrogen cycles (three times). Then, anisole (1.7 ml, 15.1 mmol), *n*-decane (150 μl), VAc (M, 4 mL, 43.2 mmol) and CCl_4 initiator (YZ, 21.2 μl, 0.2 mmol) were introduced into the flask, using a syringe, keeping a constant flow of nitrogen. The mixture was stirred for 10 min at room temperature until homogeneity was reached. At that point, 5 aliquots (1.1 mL each) of solution were injected into baked glass tubes and sealed under nitrogen. The tubes were immersed in an oil bath previously heated at 70°C. The polymerization was stopped at the desired time.

2.4. Polymer characterization

Number average molecular weight ($\overline{M_n}$) and dispersity (Đ) of the polymer samples were determined using a gel permeation chromatographer (GPC), Waters 2695 ALLIANCE Separation Module, equipped with two HSP gel columns in series (HR MBL molecular weight range from 5×10^2 to 7×10^5 and MB-B from 1×10^3 to 4×10^6) and a RI Waters 2414 detector. THF was used as eluent at 35°C with a flow rate of 0.5 mL/min. Standards of linear polystyrene were used for calibration. Polymer samples were injected into the GPC without any purification, but some samples were purified by passing the reaction mixture through an Al_2O_3 column using THF as eluent. GPC curves of the purified pVAc and the samples without purification obtained in the same experiments were very similar. Monomer conversion was determined from the concentration of residual monomer, measured by gas chromatography (GC) using a Shimadzu GC-2010 gas chromatograph equipped with one capillary column RESTEK stabilwax (30 m, 0.53 mm ID, and 0.5 μmdf), with *n*-decane as an internal standard in each polymerization. Analysis conditions: injector temperature, 220°C; temperature program: 4 min at 40°C, heating rate of 15°C/min until 220°C was reached, then 2 min at 220°C. IR spectra were recorded on a Nicolet-Magna 750 FT-IR instrument in KBr pellets. ^{1}H NMR spectra were obtained on Bruker Avance 400 MHz and Varian 300 MHz spectrometers.

3. Modeling

3.1. Polymerization scheme

The polymerization scheme used in this study, as implemented in the Predici® software of CiT, is shown in Table 1. The reactions that make up the reaction mechanism are called "steps" as in the Predici® literature.[43] Step 1 represents reversible

Table 1. Polymerization scheme for the RIR-telomerization of VAc as implemented in Predici®.

Reaction	Step	Name of step in Predici	Kinetic constant	Step #
Initiation	YZ+C ↔Y•+ZC	Reversible reaction	k_a, k_b	1
First propagation	Y•+M → P(1)	(Anionic) Initiation step	k_p	2
Propagation	P(s)+M →P(s+1)	Propagation	k_p	3
Dormant-living exchange (Activation)	PZ(s)+C→ P(s)+ZC	Change	k_{a_2}	4
Dormant-living exchange (Deactivation)	P(s)+ZC→ PZ(s)+C	Change	k_b	5
Transfer to initiator	P(s)+ YZ→PZ(s)+ Y•	Change	k_{trYZ}	6
Termination	P(s) + P(r) → D(s+r) P(s) + P(r) → D(s)+D(r)	Termination by combination and disproportionation	k_{tc}, k_{td}	7
Microwave-promoted generation of radicals	M → 2M•	Elemental	k_{ir}	8

metal-catalyzed initiation. Steps 2 to 7 account for radical telomerization, as described by Boutevin.[44]

As explained above, three modeling approaches were used to account for MI telomerization of VAc. These approaches are described below.

Model A. Microwave-induced generation of free radicals from monomer

In this model, the microwave effect is accounted for by considering the hypothetical generation of free radicals from monomer (Step 8 in Table 1). The corresponding kinetic rate constant, k_{ir}^0, is estimated for each case.

Model B. Increased reaction temperature

The temperature of the reacting mixture, T_f, is considered to be higher than the one measured experimentally. IRS devices measure temperatures on the surface of the reactor, leading to underestimation of the actual temperature.[26,29,30,45] In Predici®, it is possible to predefine temperature profiles as a function of time.[36]

Model C. Microwave-enhanced activation-deactivation

In this model, only catalyst-involved reactions are affected by MI. Kinetic rate constants k_b^0, k_a^0 and $k_{a_2}^0$ are estimated for the microwave-assisted cases (Steps 1, 4 and 5 of Table 1).

Molecular weight development was followed in terms of number-average molecular weight, $\overline{M_n}$, and dispersity of molecular weight, Đ.

3.2. Diffusion-Controlled (DC) effects

Diffusion-controlled effects were modeled using equilibrium free-volume theory.[46] Kinetic rate constants were corrected for DC-effects according to Equation 1, where k_i is an effective kinetic rate constant, and k_i^0 is the corresponding intrinsic kinetic rate constant for $i = a, a_2, b, trYZ, p, t_c, t_d \text{ and } ir$, namely, the different reactions involving polymer molecules, which may become diffusion-controlled.

$$k_i = k_i^0 \exp\left[-\beta_i\left(\frac{1}{V_f} - \frac{1}{V_{f0}}\right)\right] \quad [1]$$

V_f and V_{f0} in Equation (1) are fractional free volume at time t and at time zero, respectively, and are calculated using Equation (2). β_i are free-volume parameters.

$$V_f = 0.025 + \sum_{k=1}^{of\ components} \alpha_k\left(T - T_{gk}\right)\varphi_k \quad [2]$$

T_{gk} is the glass transition temperature of component k, α_k is expansion coefficient for species k, and φ_k is the fractional volume of component k.[46]

4. Results and discussion

Thirteen RIR-Telomerization cases were studied in the present work; eleven of them correspond to systems under CH and the other two to MI. Initial conditions for all cases are summarized in Table 2. The effects of solvent type and concentration, as well as initiator concentration on polymerization rate and molecular weight development ($\overline{M_n}$ and Đ versus conversion) were studied for the cases under CH. Models A, B, C and a combination of Models B and C (Model D) were used to analyze the cases under MI.

Table 2. Initial conditions for the RIR-telomerizations of VAc.

Case	Temperature (°C)	(M)/(YZ)/(C)	S/M (v/v)	Solvent	Microwave Power (W)	Reference
1	50	233/1/1	5/5	Ethyl acetate	0	[47]
2	70	200/0.5/1	3/7	Anisole	0	This work
3	70	200/1/1	3/7	Anisole	0	This work
4	70	200/2/1	3/7	Anisole	0	This work
5	70	200/4/1	3/7	Anisole	0	This work
6	70	200/1/1	5/5	Anisole	0	[40]
7	70	200/2/1	5/5	Anisole	0	[40]
8	70	200/2/1	3/7	Anisole	0	This work
9	70	200/1/1	5/5	DMSO	0	[40]
10	70	200/2/1	5/5	DMSO	0	[40]
11	70	100/1/1	5/5	DMSO	0	[40]
12	70	200/1/1	5/5	DMSO	100	[40]
13	70	200/1/1	5/5	DMSO	500	[40]

Table 3. Physical and kinetic parameters used in the simulations.

Parameter	Units	Value	Reference or remark
k_p^0	L mol^{-1} s^{-1}	$1.47 \times 10^7 \exp(-2490/T)$	[48]
k_t^0	L mol^{-1} s^{-1}	$2.7 \times 10^{10} \exp(-1400/T)$	[49]
$C_{YZ} = \frac{k_p}{k_{trYZ}}$	Dimensionless	1	[50]
T_{gm}, T_{gp}, T_{gs}	°C	−150, 30, −160	This work,[51] this work
α_m, α_p, α_s	Dimensionless	1×10^{-3},4.8×10^{-4}, 7×10^{-3}	[36] (Assumed the same as MMA)
β_p, β_t	Dimensionless	1.02, 3.3	This work
β_a, β_b, β_{a_2}	Dimensionless	0.2,0.5, 0.2	[36]
E_a / R, E_b / R, E_{a_2} / R	K	1600,1600, 2100	This work

4.1. RIR-Telomerization of VAc by CH

The model for redox-initiated radical telomerization of VAc was first validated with experimental data for VAc in ethyl acetate (EtOAc), anisole and dimethyl sulfoxide (DMSO), carried out by CH. The kinetic rate constants and physicochemical parameters used in the simulations are listed in Table 3. Free volume parameters for the propagation and termination reactions, β_p and β_t, respectively, were estimated from the bulk polymerization of VAc using AIBN at 70 °C[42]; β_a, β_b and β_{a_2} were assumed to take the values used in the ATRP of styrene using ethyl 2-bromopropionate (EBP), copper bromide (CuBr), and N,N,N′,N′,N″-pentamethyldiethylenetriamine (PMDETA).[36]

4.1.1. Redox-initiated radical telomerization of VAc in EtOAc at 50 °C by CH

Case 1 deals with the RIRT of VAc using iron oxyacetate $Fe(OAc)_2$ / PMDETA (N,N,N′,N′,N″- pentamethyl diethylene triamine) and CCl_4, at 50 °C, in EtOAc.[47] Three kinetic rate constants, namely, k_b^0, k_a^0 and $k_{a_2}^0$ were fitted to the available experimental data. Parameters are reported in Table 4. Figure 1 shows the calculated and experimental profiles of (a) ln (M_0 / M) versus t(h), (b) $\overline{M_n}$ versus conversion, and (c) Đ versus conversion. It is observed in Figure 1 that the agreement between experimental and calculated profiles is very good. The expected main features of RIR-telomerizations are captured by the model, namely: (a) existence of limiting conversions, (b) relatively constant $\overline{M_n}$ versus conversion profiles, and c) Đ = 2 throughout the reaction.

4.1.2. Redox-initiated radical telomerization of VAc in anisole by CH at 70 °C

Cases 2 to 8 correspond to polymerization of VAc at 70 °C with $(Ru(\eta^6\text{-}C_6H_6)(C_6H_4\text{-}2\text{-}H_2NMe_2)(MeCN))PF_6$, (**1**) and CCl_4. Cases 2–5 and 8 correspond to RIR-telomerizations with M/S = 3/7 (v/v). The polymers were synthesized following the experimental procedure described by Olvera-Mancilla et al.[40] Cases 6 and 7, on the other hand, correspond to RIR-telomerizations with M/S = 5/5 (v/v).[40] Case 3 was used to estimate kinetic rate constants k_b^0, k_a^0 and $k_{a_2}^0$ (see Table 4). The calculated profiles of (a) ln (M_0 / M) versus time, (b) $\overline{M_n}$ versus conversion and (c) Đ versus conversion for Cases 2 to 5 are shown in Figure 2. The corresponding profiles for Cases 6 and 7 are shown in Figure 3.

The effect of initiator initial concentration is addressed in Cases 2 to 5. The initial concentration of initiator increases from Case 2 to 5. As expected, the highest polymerization rate of is observed with Case 5, whereas that the lowest one is obtained with Case 2 (see Figure 2a). $\overline{M_n}$ decreases as initiator concentration is increased, as observed in Figure 2b, and Đ is slightly decreased as initiator concentration is increased (Figure 2c). Similar results were obtained for Cases 6 and 7. It

Table 4. Estimated kinetic rate constants and T_f for Cases 1 to 13.

Case	k_b^0 (L mol^{-1} s^{-1}) [¥]	k_a^0 (L mol^{-1} s^{-1}) [¥]	$k_{a_2}^0$ (L mol^{-1} s^{-1}) [¥]	k_{tr}^0 (s^{-1})	T_f (°C)
1	2×10^4	8×10^{-3}	1×10^{-4}	—	—
2 to 8	1.5×10^7	4×10^{-3}	2×10^{-4}		
9–11[f]:	2×10^6	6×10^{-3}	1×10^{-4}		
12-A[f]:	2×10^6	6×10^{-3}	1×10^{-4}	2×10^{-8}	—
13-A[f]:	2×10^6	6×10^{-3}	1×10^{-4}	5×10^{-8}	—
12-B[f]:	2×10^6	6×10^{-3}	1×10^{-4}	—	105
13-B[f]:	2×10^6	6×10^{-3}	1×10^{-4}	—	130
12-C[f]:	3×10^7	3×10^{-1}	3×10^{-1}	—	—
13-C[f]:	3×10^6	5×10^{-2}	5×10^{-2}	—	—
12-D[f]:	3×10^7	9×10^{-2}	9×10^{-2}	—	90
13-D[f]:	3×10^6	7×10^{-3}	7×10^{-3}	—	115
9–11 [g]:	2×10^6	2×10^{-3}	1×10^{-4}		
12-A[g]:	2×10^6	2×10^{-3}	1×10^{-4}	2×10^{-8}	—
13-A[g]:	2×10^6	2×10^{-3}	1×10^{-4}	5×10^{-8}	—
12-B[g]:	2×10^6	2×10^{-3}	1×10^{-4}	—	120
13-B[g]:	2×10^6	2×10^{-3}	1×10^{-4}	—	150
12-C[g]:	3×10^7	3×10^{-1}	3×10^{-1}	—	—
13-C[g]:	3×10^6	5×10^{-2}	5×10^{-2}	—	—
12-D[g]:	3×10^7	6×10^{-2}	6×10^{-2}	—	105
13-D[g]:	3×10^6	4×10^{-3}	4×10^{-3}	—	135

[¥]Fitted values at initial reaction temperatures of 50 °C for Case 1 and 70 °C for Cases 2 to 13.
[f]:Fitted values with $C_{YZ} = 1$.
[g]:Fitted values with $C_{YZ} = 3$

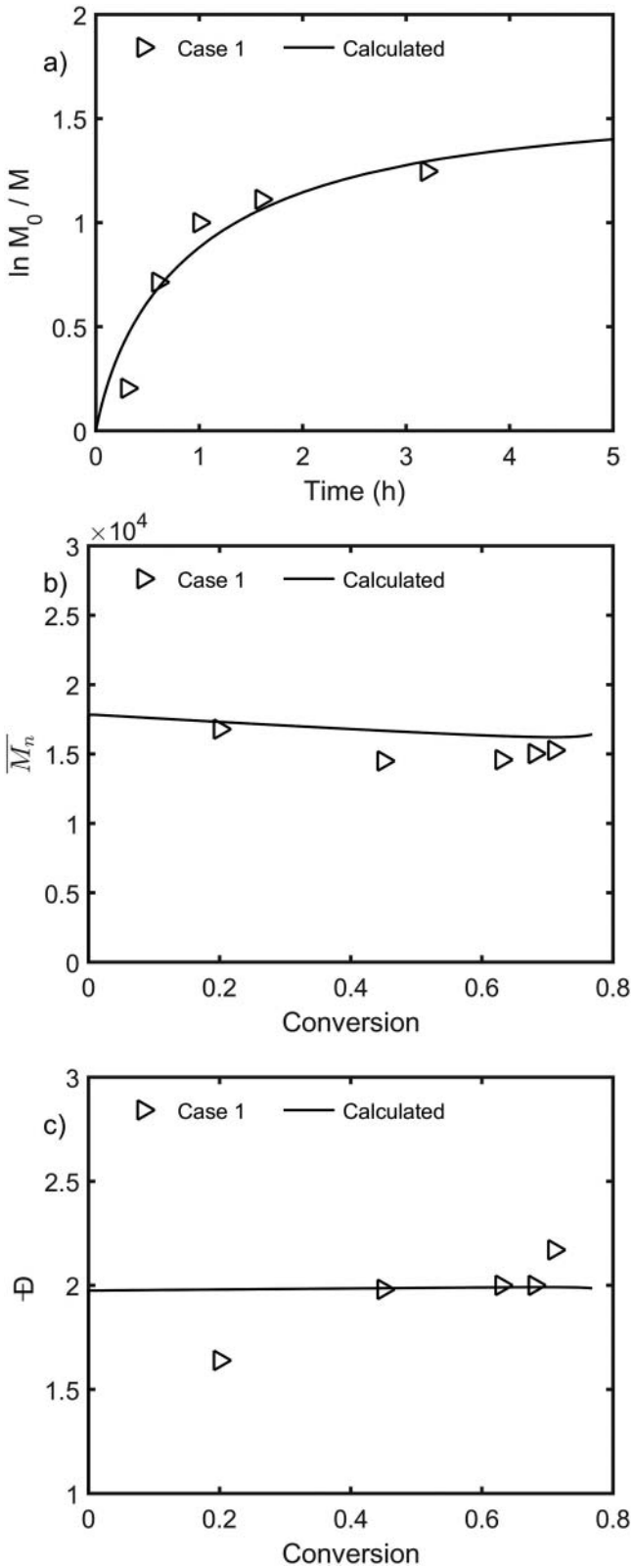

Figure 1. Comparison of calculated and experimental profiles for RIR-Telomerization of VAc in EtOAc at 50 °C under CH: (a) ln (M_0/M) versus time, (b) $\overline{M_n}$ (g mol^{-1}) versus conversion and (c) Đ versus conversion.

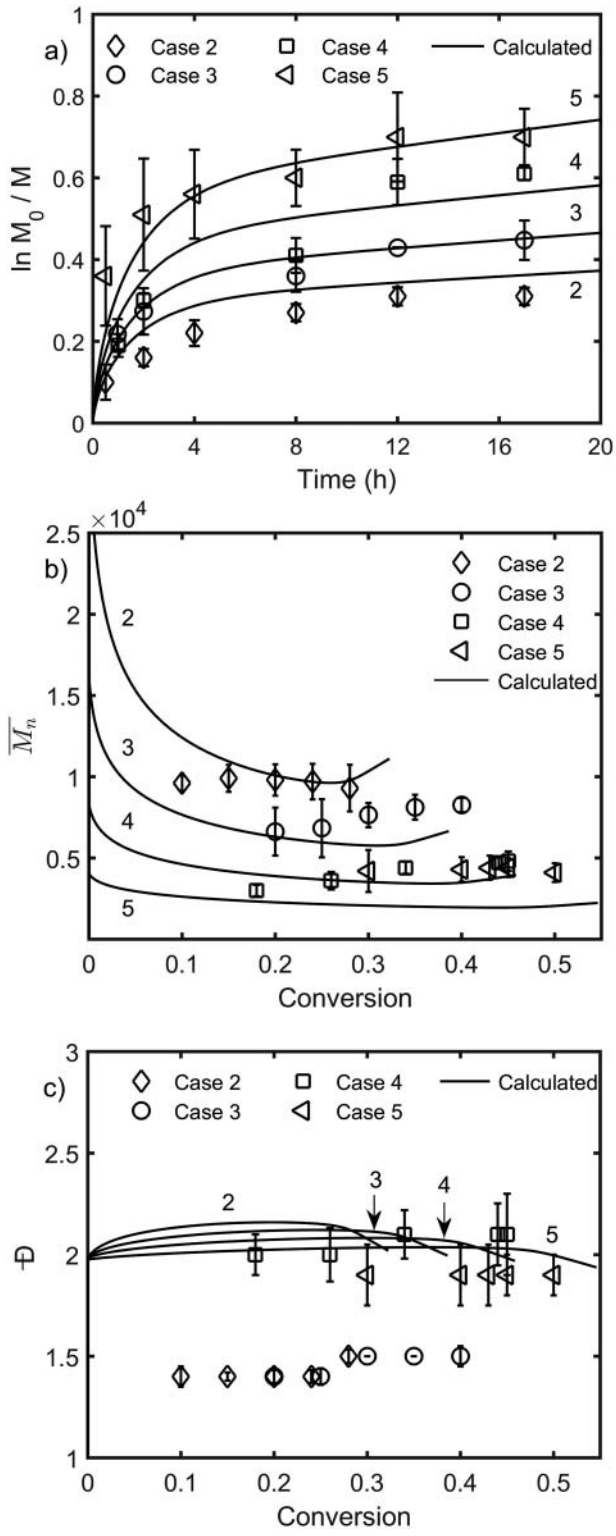

Figure 2. Comparison of calculated and experimental profiles for CH RIR-Telomerization of VAc in DMSO at 70 °C for Cases 2 to 5: (a) ln (M_0/M) versus time, (b) $\overline{M_n}$ (g mol^{-1}) versus conversion and (c) Đ versus conversion.

is observed in Figure 2c that experimental Đs take values around 1.5 for Cases 2 and 3, and Đ ≈2 for Cases 4 and 5. This discrepancy between experimental and calculated values of Đ for Cases 2 and 3 may be attributed to experimental error. For instance, Cases 4 and 8 are replicates (see the corresponding entries in Table 2) whose experimental and calculated ln (M_0/M) vs. time, $\overline{M_n}$ vs. conversion and Đ vs. conversion profiles are compared in Figure 4. It is observed in Figure 4c that Đ≈2 for Case 4 and Đ≈1.5 for Case 8. The agreement between calculated and experimental profiles is very good in Case 4, for conversion and molecular weight development.

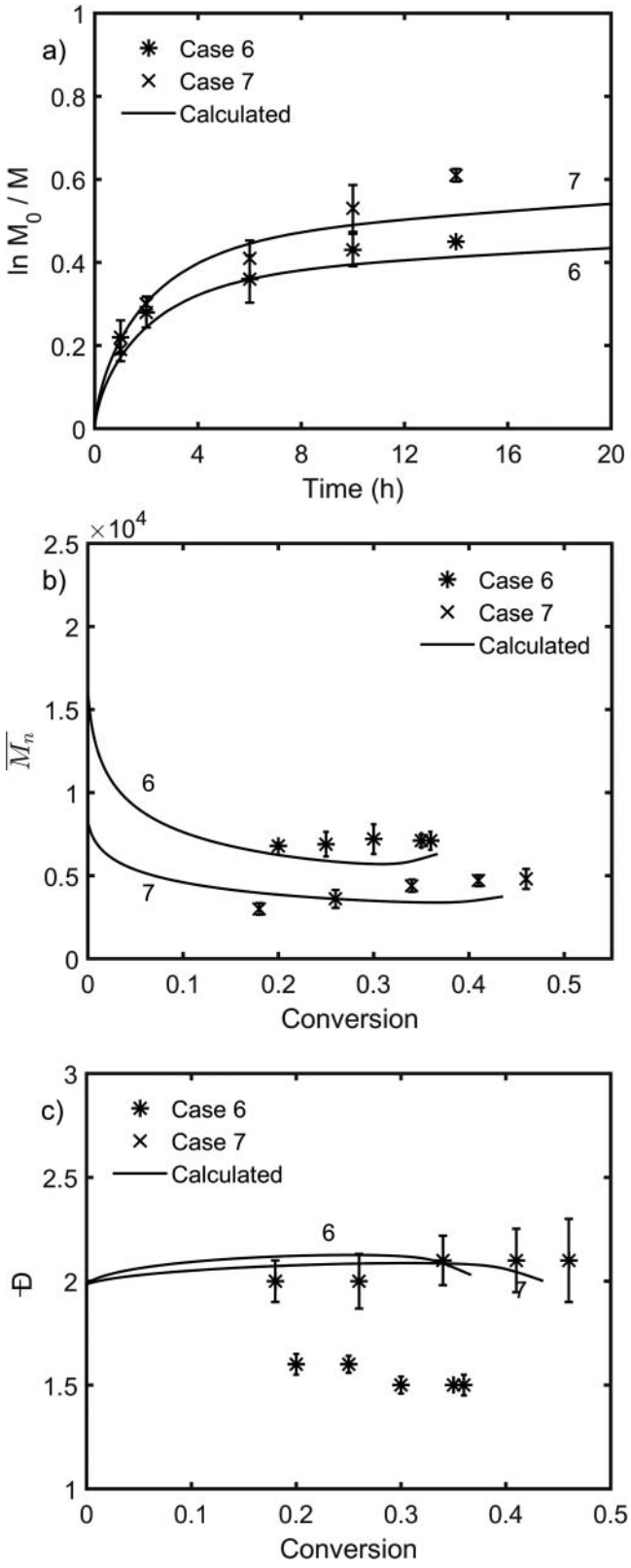

Figure 3. Comparison of calculated and experimental profiles for CH RIR-Telomerization of VAc in anisole for Cases 6 and 7: (a) ln (M_0/M) versus time, (b) $\overline{M_n}$ (g mol^{-1}) versus conversion and (c) Đ versus conversion.

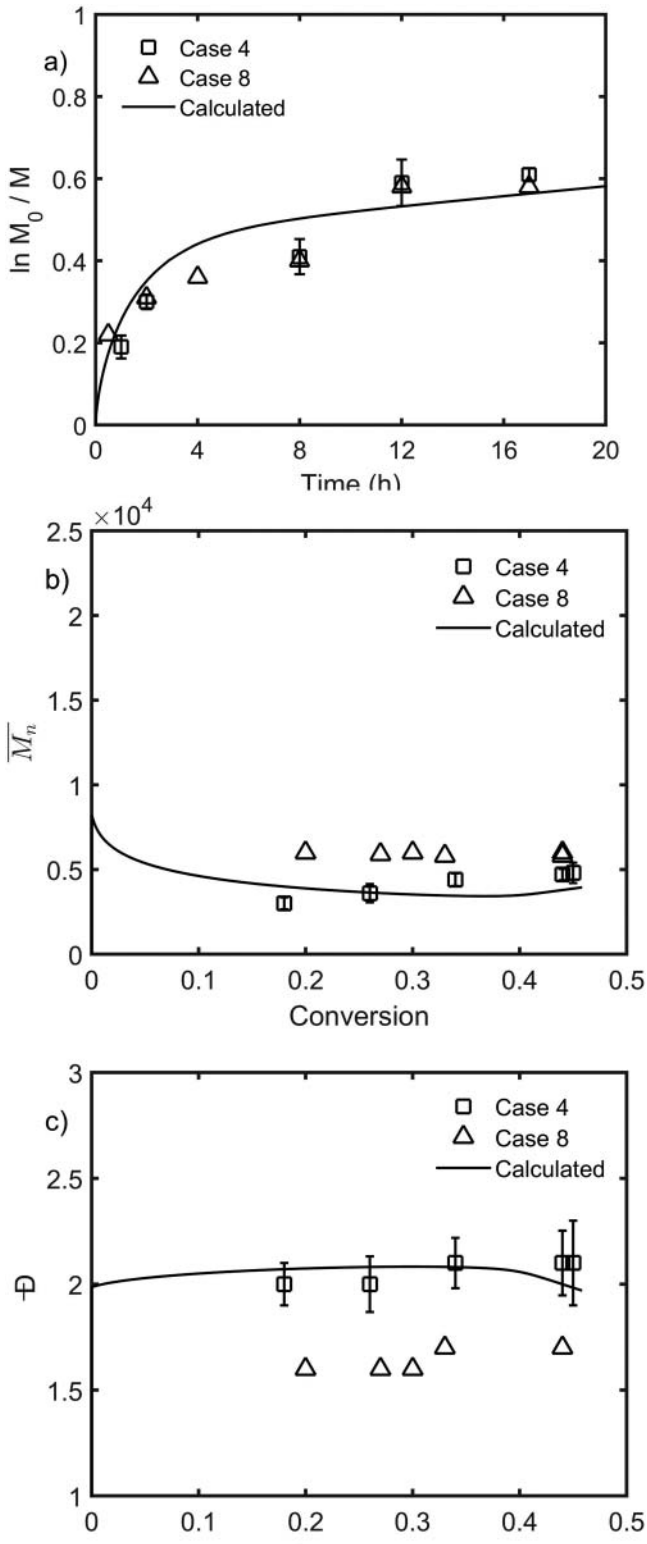

Figure 4. Comparison of calculated and experimental profiles for CH RIR-Telomerization of VAc in anisole for Cases 4 and 8 (replicate): (a) ln (M_0/M) versus time, (b) $\overline{M_n}$ (g mol^{-1}) versus conversion and (c) Đ versus conversion.

4.1.3. Redox-initiated radical telomerization of VAc in DMSO at 70 °C under CH

Cases 9 to 11 in Table 2 represent the redox-initiated radical telomerization of VAc, using CCl_4 and catalyst **1**, in DMSO, at 70 °C. Case 9 was used to estimate parameters k_b^0, k_a^0 and $k_{a_2}^0$ (see Table 3). Simulation results for polymerization rate, expressed as ln (M_0/M) versus time, and molecular weight development ($\overline{M_n}$ and Đ versus conversion) are shown in Figure 5. Calculated logarithmic conversion agrees well with experimental data during the early stages of the reaction (see

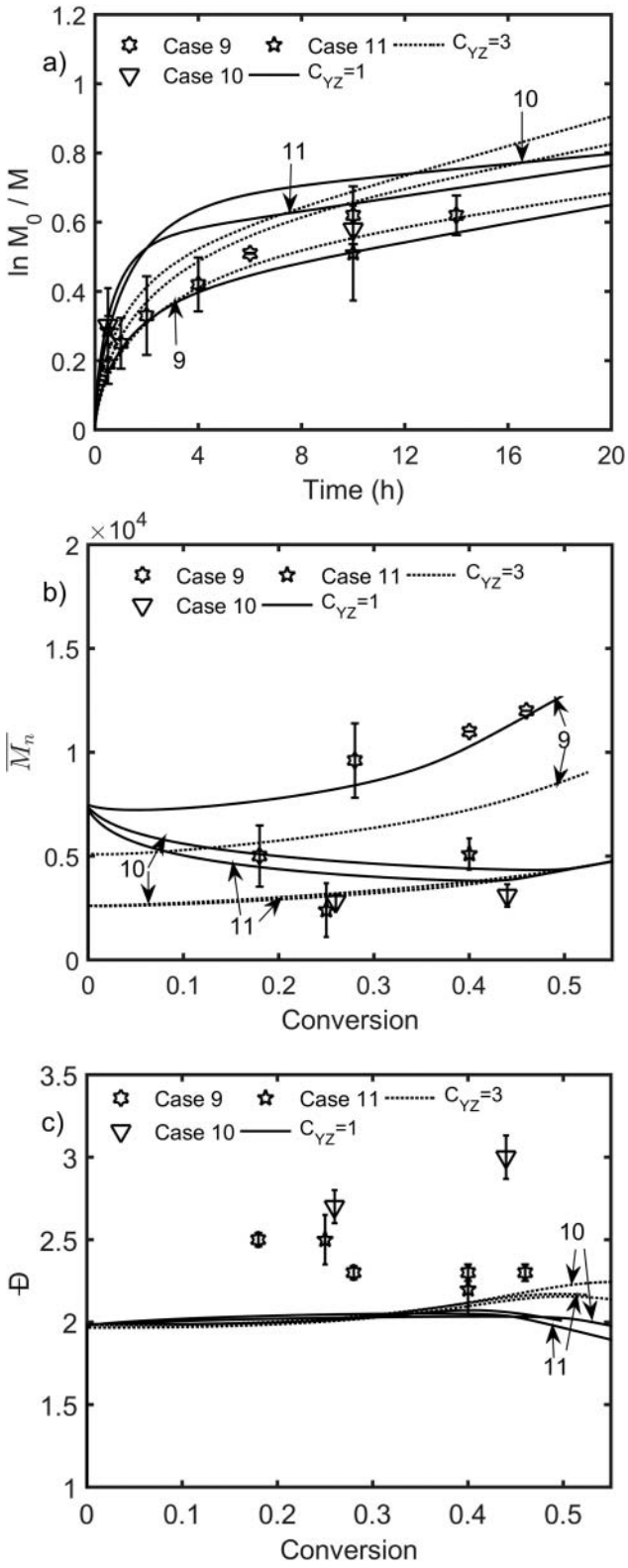

Figure 5. Comparison of predicted profiles and experimental data for CH RIR-Telomerization of VAc in DMSO at 70 °C for Cases 9 to 11 with $C_{YZ} = 1$ and $C_{YZ} = 3$: (a) ln $(M_0 \ / \ M)$ versus time, (b) $\overline{M_n}$ (g mol^{-1}) versus conversion, and (c) Đ versus conversion.

Figure 5a). However, large deviations are observed after 8 hours of reaction, especially for Cases 10 and 11. It is not clear in Figure 5b if the experimental profile of $\overline{M_n}$ versus conversion is linear or not. Our model calculations clearly show a nonlinear

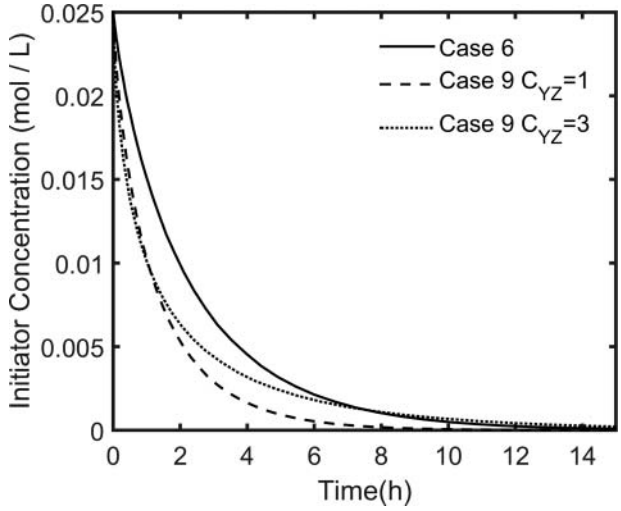

Figure 6. Predicted initiator concentration profile for CH RIR-Telomerization of VAc in Anisole (Case 6), and in DMSO (Case 9), with $C_{YZ} = 1$ & 3 , at 70 °C.

trend, which may be caused by the dominance of conventional free radical behavior at the early stages of the polymerization. Specifically, in Case 9 the profile seems to be linear, but if the first experimental data point is suppressed (a possible outlier) the experimental trends would coincide with the calculated ones. The predicted profiles of Đ versus conversion almost overlap at a value of Đ≈2, whereas the experimental values lie between 2.2 and 2.5, with the exception of Case 10, which clearly shows a deviated increasing trend.

Olvera-Mancilla et al.[40] reported that CCl_4 consumption was faster in DMSO than in other solvents (anisole, DMF, MEK), suggesting that telomerization reactions involving CCl_4 (steps 1 & 6 in Table 1) are affected by the solvent.

It was assumed in our simulations that the chain transfer to CCl_4 constant, defined as $C_{YZ} = \frac{k_{trYZ}}{k_p}$, is equal to one.[45] The only kinetic rate constants that had in principle to be estimated in this case were the ones related to the activation and deactivation steps (k_a^0, k_b^0, and $k_{a_2}^0$). Although values of $C_{YZ} \geq 3$ were found to describe the evolution of $\overline{M_n}$ during the early stages of telomerization, overestimation is observed at intermediate and high conversions, as shown in Figure 5. CCl_4 in DMSO and anisole concentration profiles are presented in Figure 6. It is observed that the consumption of CCl_4 is faster in DMSO than in anisole. It is slightly faster when $C_{YZ} = 3$, compared to the case with $C_{YZ} = 1$ during the first hour of reaction, and later it turns out to be faster when $C_{YZ} = 1$. This is explained by the fact that the fitted value of $k_a^0 = 6 \times 10^{-3} (C_{YZ} = 1) > k_a^0 = 2 \times 10^{-3} (C_{YZ} = 3)$, that is, transfer to CCl_4 is initially favored (Step 6), but after the consumption of CCl_4 initiation is dominant (Step 1).

4.2. Radical telomerization of VAc in DMSO by MI

Olvera-Mancilla et al.[40] found that MI polymerizations of VAc were unsuccessful in solvents of low dielectric constants such as anisole ($\varepsilon = 4.3$) and methyl ethyl ketone (MEK, $\varepsilon = 18.5$) but proceeded well in highly polar solvents, such as dimethyl sulfoxide (DMSO, $\varepsilon = 46.7$) and N, N-dimethylformamide (DMF, $\varepsilon = 38$), using (Ru(η^6-C_6H_6)(C_6H_4-2-H_2NMe_2)(MeCN))PF_6 (**1**) as catalyst. However, polymerizations were also unsuccessful when other catalysts, such as (Ru(*o*-C_6H_4-2-

py)(MeCN)$_4$)PF$_6$ (**2**) and (Ru(η^6-C$_6$H$_6$)(*o*-C$_6$H$_4$-2-py)Cl),[3] were used.

Models A, B and C (section 2.1) were conceived to study these systems. Specifically, the MI RIR-telomerization of VAc/**1** in DMSO (Cases 12 and 13) is addressed here. Results are compared to the corresponding system under CH (Case 9 of Table 2).

The calculated profiles of (a) ln (M_0 / M) versus time, (b) $\overline{M_n}$ versus conversion and (c) Đ versus conversion are shown in Figures 7 (for Models A and B) and 8 for Model C. The estimated parameters for each model are presented in Table 4: k^0_{ir} for Model A, T_f for Model B, and k^0_b, k^0_a and $k^0_{a_2}$ for Model C.

4.2.1. Use of Model A for Cases 12 and 13

The values of k^0_{ir} estimated for Cases 12 and 13 (2×10^{-8} and 5×10^{-8} s^{-1}, respectively) are comparable in magnitude to the corresponding parameter used in the MI ATRP of methyl methacrylate at 69 °C and 360 W of irradiation power ($k^0_{ir} = 2\times10^{-8}$ s^{-1}, Simulation 2a in[36]). The agreement between calculated and experimental profiles of ln(M_0/M) versus time is very good for Case 12, but there is significant disagreement in Case 13, as observed in Figure 7. The calculated values of $\overline{M_n}$ for Cases 12 and 13 follow a fairly constant trend during most of the conversion range, and are higher than the corresponding values calculated for Case 9. However, the experimental data of M_n versus conversion deviate significantly from the calculated profiles, particularly in Case 12. The calculated Đ values were about 2 in all cases, with very good agreement for Case 12, but significant deviation in the low to intermediate conversion ranges.

4.2.2. Use of Model B for Cases 12 and 13

Reaction temperatures of $T_f = 105\ ^\circ C$ and $T_f = 140\ ^\circ C$ were used with Model B for Cases 12 and 13, respectively. It is interesting to note that these temperatures are lower than the one used for MI-ATRP of MMA using 360 W of irradiation power ($T_f = 215\ ^\circ C$, Simulation 2c in[36]). Activation energies for the initiation, activation and deactivation reactions (Steps 1, 4 and 5 in Table 1) were assigned reasonable order of magnitude values (Table 3). Results are shown in Figure 7. The calculated logarithmic conversion versus time profile agrees well with experimental data. The $\overline{M_n}$ versus conversion profiles decrease slightly with conversion and the Đ values are similar in all cases (Đ≈2). Once again, the agreement between predictive profiles and experimental data for M_n and Đ versus conversion is poor for Cases 12 and 13.

4.2.3. Use of Model C for Cases 12 and 13

Three kinetic rate constants, k^0_b, k^0_a, and $k^0_{a_2}$, are involved in Model C. The estimated values of these parameters for Cases 12 and 13 were the following: $k^0_b = 3\times10^7$ L mol^{-1} s^{-1}, $k^0_a = k^0_{a_2} = 3\times10^{-1}$ L mol^{-1} s^{-1}, and $k^0_b = 3\times10^6$ L mol^{-1} s^{-1}, $k^0_a = k^0_{a_2} = 5\times10^{-2}$ L mol^{-1} s^{-1}, respectively. As observed in Figure 8, there is fairly good agreement between calculated and experimental profiles of $ln(M_0/M)$ versus time (Figure 8a). In the case of M_n versus conversion, the agreement is good for Cases 9 and 12, but poor for Case 13 (see Figure 8b). Unfortunately, the improved behavior in the description of molecular weight development obtained in this case, compared to the predictions of Models A and B, was not observed in the case of Đ versus conversion, where higher deviations were obtained, particularly for Case 12 (see Figure 8c).

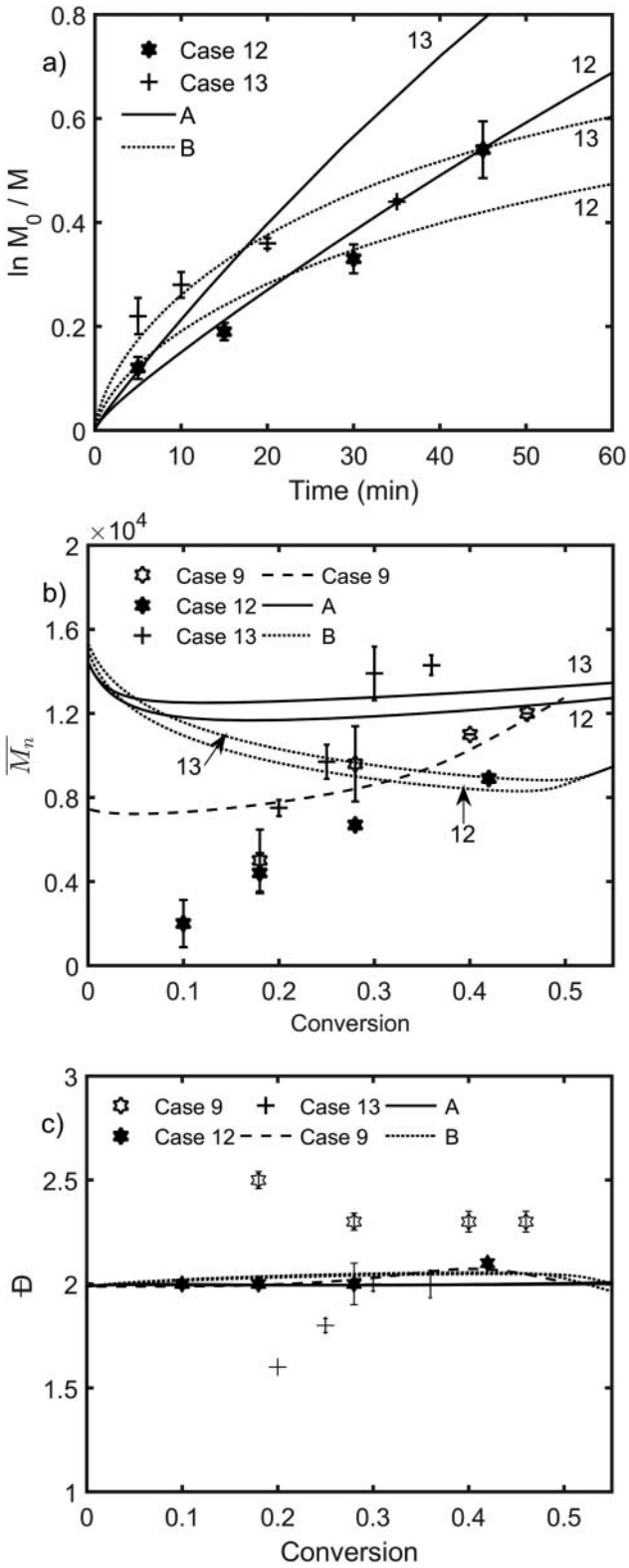

Figure 7. Comparison of calculated profiles and experimental data of MI RIR-Telomerization of VAc in DMSO using Models A and B for Cases 12 and 13, with $C_{YZ} = 1$: (a) ln (M_0 / M) versus time, (b) $\overline{M_n}$ (g mol^{-1}) versus conversion, and (c) Đ versus conversion. Case 9 is included in (b) and (c) for comparison purposes.

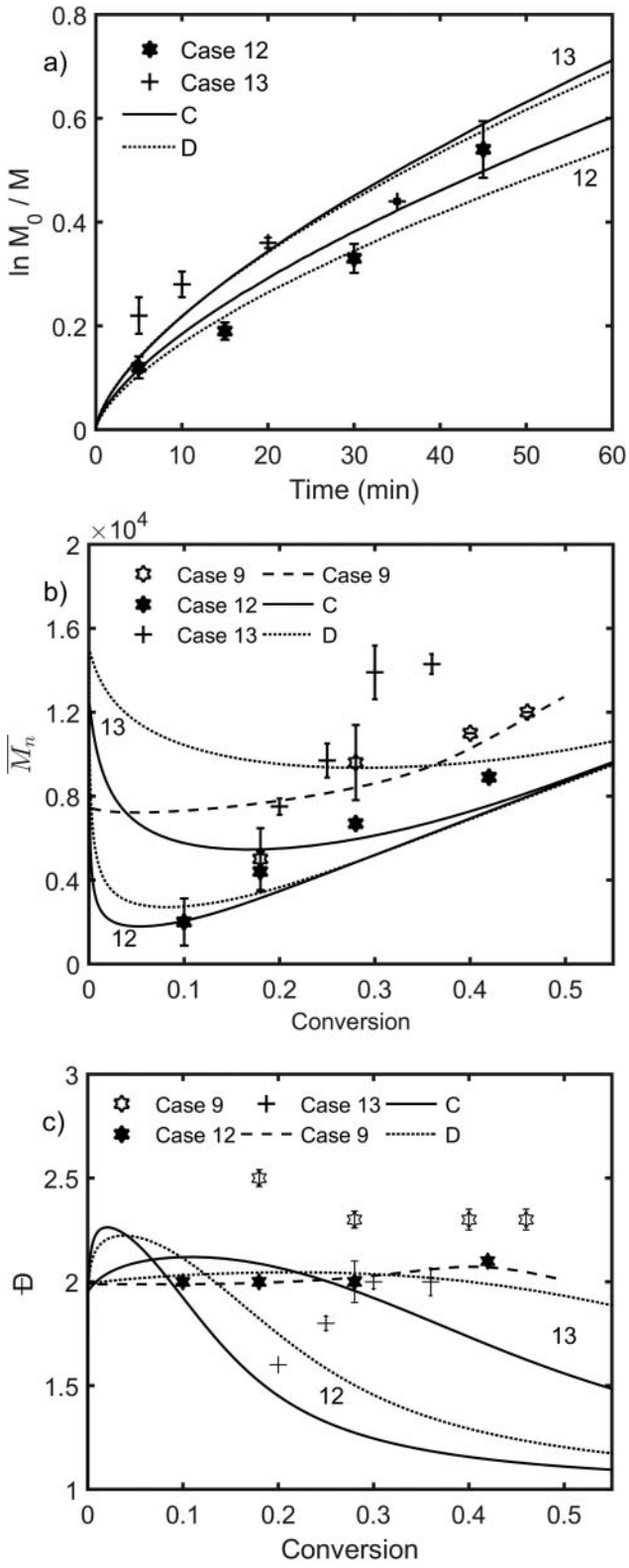

Figure 8. Comparison of calculated profiles and experimental data of MI RIR-Telomerization of VAc in DMSO using Models C and D for Cases 12 and 13 using $C_{YZ} = 1$: (a) ln $(M_0 \ / \ M)$ versus time, (b) $\overline{M_n}$ (g mol^{-1}) versus conversion, and (c) Đ versus conversion. Case 9 is included in (b) and (c) for comparison purposes.

4.2.4. Use of combined models B and C (Model D) for cases 12 and 13

Model D consisted of the combination of Models B and D. For our calculations using model D, a value of T_f lower than the one used in Model B was chosen, and then kinetic rate constants k_b^0, k_a^0 and $k_{a_2}^0$ were estimated. The values used for these four parameters are summarized in Table 4. As observed in Figure 8, the results obtained did not changed significantly from the calculations using Model C.

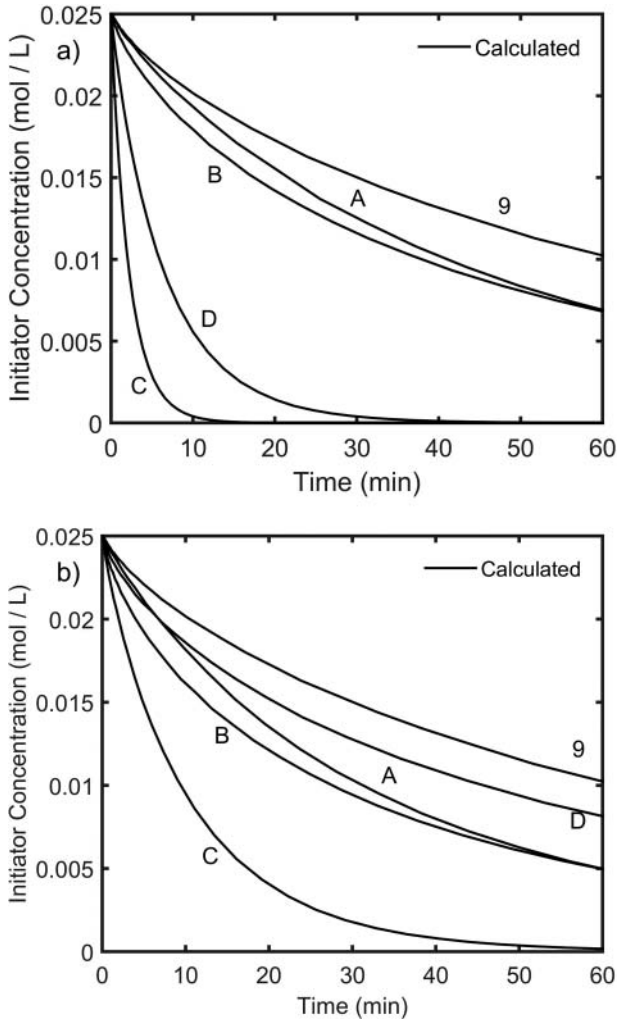

Figure 9. Calculated profiles of initiator (CCl_4) concentration, using Models A to D for (a) Case 12, and (b) Case 13, using $C_{YZ} = 1$. Case 9 is shown for comparison purposes.

Olvera-Mancilla et al.[40] observed that total consumption of CCl_4 by MI occurred after the first 3 min of reaction, as measured by GC. In Figure 9, the calculated profiles of initiator concentration versus time are shown. The fastest initiator consumption occurs with Model C (10 min), followed by Model D (30 min), for Case 12, whereas that the fastest consumption for Case 13 also occurs with Model C (40 min), followed this time by Model B.

Table 5. $\overline{M_n}$ and Đ as a function of conversion.

Model	Case 12 $\overline{M_n}$	Case 13 $\overline{M_n}$	Case 12 Đ	Case 13 Đ
A	Constant	Constant	≈ 2	≈ 2
B	Slightly linear decrease	Slightly linear decrease	≈ 2	≈ 2
C	Increase linearly	Constant	Decrease	Decrease
D	Increase linearly	Constant	Decrease	Decrease

4.2.5. Main features of Models A to D with $C_{YZ} = 1$

Models A to D can effectively describe the observed increase in polymerization rate for Cases 12 and 13. The linear increase of $\overline{M_n}$ with conversion is adequately predicted by Model C for Cases 12 and 13. As a result, low values of $Đ$ are obtained at moderate and high conversions. The dependence of $\overline{M_n}$ and $Đ$ with conversion is summarized in Table 5. The best match with experimental data of $\overline{M_n}$ is obtained with Model D for Cases 12

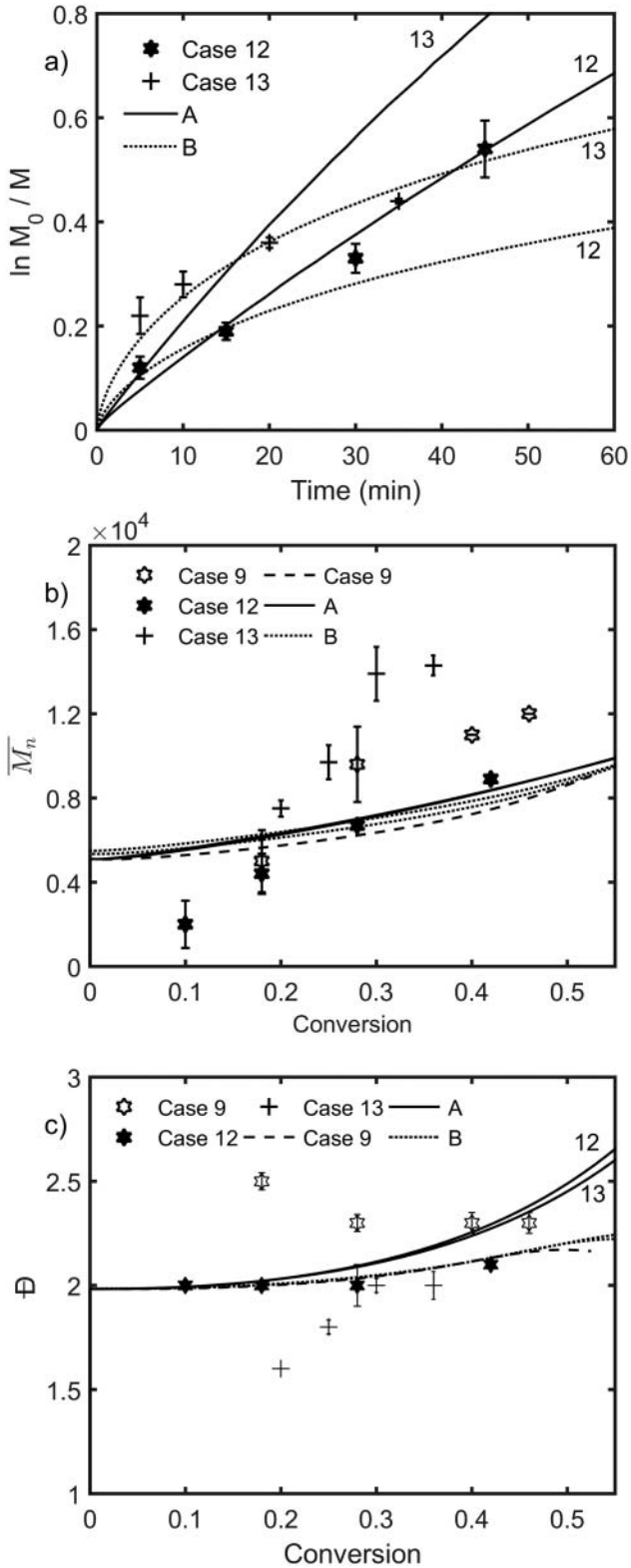

Figure 10. Comparison of calculated profiles and experimental data of MI RIR-Telomerization of VAc in DMSO using Models A and B for Cases 12 and 13 using $C_{YZ} = 3$: (a) ln $(M_0 \ / \ M)$ versus time, (b) $\overline{M_n}$ (g mol^{-1}) versus conversion, and (c) Đ versus conversion. Case 9 is included in (b) and (c) for comparison purposes.

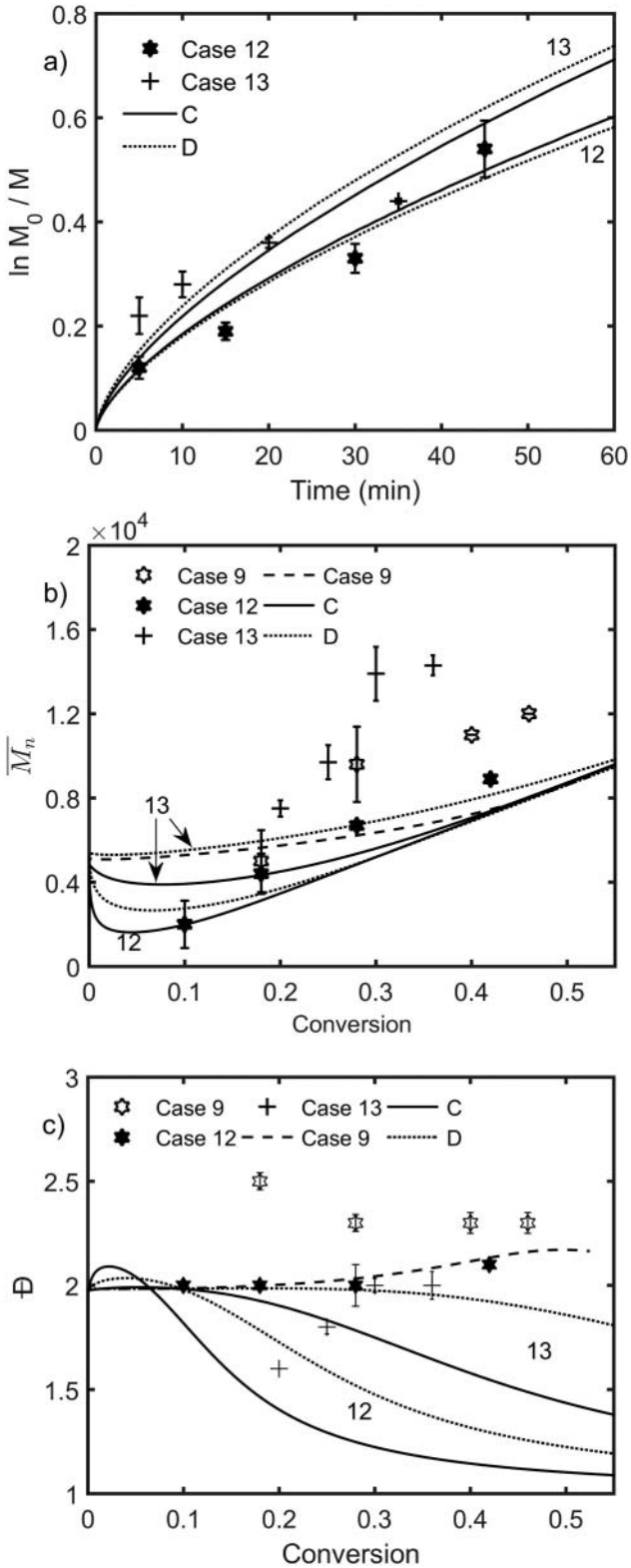

Figure 11. Comparison of calculated profiles and experimental data of MI RIR-Telomerization of VAc in DMSO using Models C and D for Cases 12 and 13 using $C_{YZ} = 3$: (a) ln $(M_0 \ / \ M)$ versus time, (b) $\overline{M_n}$ (g mol^{-1}) versus conversion, and (c) Đ versus conversion. Case 9 is included in (b) and (c) for comparison purposes.

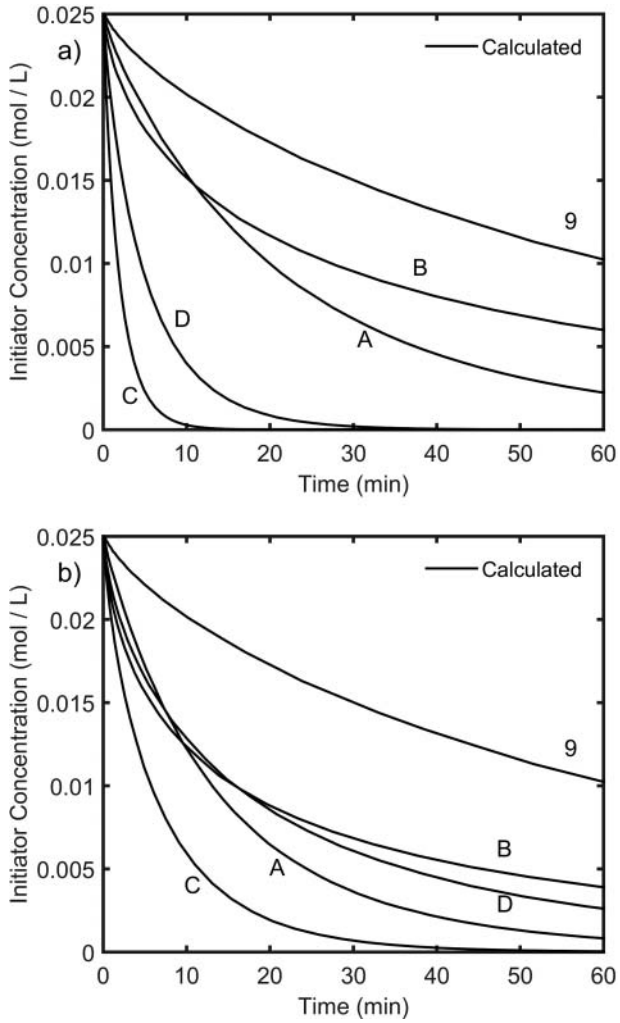

Figure 12. Calculated profiles of initiator concentration, CCl_4, using Models A to D for (a) Case 12, and (b) Case 13, using $C_{YZ} = 3$. Case 9 is shown for comparison purposes.

and 13, while that the description of $Đ$ is well represented by Models A and B for Case 12 and Model D for Case 13.

4.2.6. Simulations using $C_{YZ} = 3$

Figures 10 to 12 show the results obtained for polymerization rate, molecular weight development, and initiator consumption, using Models A, B, C and D, if $C_{CCl_4} = 3$. In general terms, slightly better agreement between calculated profiles and experimental data of polymerization rate, less variation between M_n profiles between Cases 12 and 13, and faster initiator consumption (better agreement with observed experimental results) are obtained when $C_{CCl_4} = 3$.

5. Conclusions

A kinetic model for the redox-initiated radical telomerization of vinyl acetate in which the effect of microwave heating on the properties of the components of the reaction mixture is analyzed and compared to conventional heating, was implemented in the commercial software Predici®. The kinetic model captures well the effect of initiator (CCl_4), catalyst (metal transition complexes) and solvent (ethyl acetate, anisole and DMSO) contents, as well as the absence (Cases 1 to 11) or presence of microwave irradiation (Cases 12 and 13), on polymerization rate, evolution of number-average molecular weight, $\overline{M_n}$, and dispersity of molecular weight, Đ. A limiting monomer conversion was observed whereas $\overline{M_n}$ and Đ remained relatively constant throughout the polymerization. Also, it was qualitatively demonstrated with calculations that the consumption of CCl_4 is faster in DMSO than in anisole, as reported previously from experimental evidence.[40]

Four approaches based on the "microwave" (Models A, C & D) and/or "thermal" (models B and D) effects were used to study the cases under microwave irradiation. Model A assumes microwave-induced generation of radicals from monomer. Model B considers higher reaction temperatures than those reported in the experiments. Model C assumes that microwave radiation affects specifically catalyst-involved reactions. Finally, Model D is a combination of Models B and C.

Two cases of telomerization of vinyl acetate irradiated with 100 and 500 W (Cases 12 and 13, respectively) in DMSO were addressed and contrasted with a blank reference system (Case 9). Calculations of polymerization rate calculated with either of Models A to D agreed well with the available experimental data. Different profiles of $\overline{M_n}$ versus conversion were obtained. The application of Model C showed a linear increase with conversion only for Case 12, but this approach underestimated the values of $Đ$ in the intermediate and high conversion ranges. The best agreement between experimental and calculated times for initiator (CCl_4) total consumption was obtained with Model C (3[40] and 12 minutes, respectively).

A chain transfer to CCl_4 constant C_{YZ} greater than 3 was used in the telomerizations carried out in DMSO. The use of this assumption allowed us to improve the agreement between experimental and calculated profiles of $\overline{M_n}$ versus conversion. However, underestimated profiles were predicted with Models C and D at conversions higher than 0.3.

Overall, the best results obtained in this paper were obtained with Models C and D, which suggest that microwave irradiation affects catalyst activities and/or temperature gradients were produced throughout the reaction.

Acknowledgments

The financial support from Consejo Nacional de Ciencia y Tecnología (CONACYT, Mexico, Projects CB 239364, PEI 220695 and FIT 235803, as well as the Ph.D. scholarship granted to P.L.-D.), DGAPA-UNAM (Project PAPIIT IG100815), and FQ-UNAM (PAIP 5000–9078 research budget for E.V.-L.), is gratefully acknowledged. Partial sabbatical support to E. V.-L. from the University of Ottawa, through its Distinguished Visiting Researcher Program (DVRP), during the planning of this research, is also acknowledged.

Nomenclature

C	Catalyst
C_{YZ}	Transfer constant to initiator
$D(s)$	Dead polymer molecule of size s
E_a / R	Activation energy for the activation/initiation reaction
E_b / R	Activation energy for the deactivation reaction
E_{a_2} / R	Activation energy for the activation reaction
k_a	Kinetic rate constant for the initiation/activation reaction

k_b	Kinetic rate constant for the deactivation reaction
k_{a_2}	Kinetic rate constant for the activation reaction
k_{ir}	Kinetic rate constant for microwave activation
k_p	Kinetic rate constant for the propagation reaction
k_t	Kinetic rate constant for termination by combination reaction
k_{trYZ}	kinetic rate constant for chain transfer to initiator reaction
M	Monomer
$P(s)$	Free living polymer radical of size s
$PZ(s)$	Telomer (dormant polymer) of size s
T_f	Bulk temperature
YZ	telogen or initiator

Funding

Consejo Nacional de Ciencia y Tecnología CB 239364, PEI 220695, FIT 235803
Dirección General de Asuntos del Personal Académico, Universidad Nacional Autónoma de México PAPIIT IG100815
Facultad de Química, Universidad Nacional Autónoma de México PAIP 5000-9078
University of Ottawa
Distinguished Visiting Researcher Program (DVRP)

References

[1] Bogdal, D. In *Polymer Science: A comprehensive reference*; Matyjaszewski, K., Möller, M., Eds. Elsevier: Amsterdam, **2012**; Vol. 4, pp 981–1027.
[2] Komorowska-Durka, M.; Dimitrakis, G.; Bogdal, D.; Stankiewicz, A. I.; Stefanidis, G. G. *Chem. Eng. J.* **2015**, *264*, 633–644.
[3] Sosnik, A.; Gotelli, G.; Abraham, G. A. *Prog. Polym. Sci.* **2011**, *36*, 1050–1078.
[4] De la Hoz, A.; Loupy, A. *Microwaves in Organic Synthesis*, 3rd ed.; Wiley-VCH: Weinheim, **2012**.
[5] Kempe, K.; Becer, C. R.; Schubert, S. U. *Macromolecules* **2011**, *44*, 5825–5842.
[6] Mallakpour, S.; Rafiee, Z. *Prog. Polym. Sci.* **2011**, *36*, 1754–1765.
[7] Adlington, K.; Jones, G. J.; Harfi, J. E.; Dimitrakis, G.; Smith, A.; Kingman, S. W.; Robinson, J. P.; Irvine, D. J. *Macromolecules* **2013**, *46*, 3922–3930.
[8] Nguyen, N. T.; Greenhalgh, E.; Kamaruddin, M. J.; Harfi, J. E.; Carmichael, K.; Dimitrakis, G.; Kingman, S. W.; Robinson, J. P.; Irvine, D. J. *Tetrahedron* **2014**, *70*, 996–1003.
[9] Yamada, S.; Takasu, A.; Takayama, S.; Kawamura, K. *Polym. Chem.* **2014**, *5*, 5283–5288.
[10] Matyjaszewski, K.; Tsarevsky, N. V. *J. Am. Chem. Soc.* **2014**, *136*, 6513–6533.
[11] Nicolas, J.; Guillaneuf, Y.; Lefay, C.; Bertin, D.; Gigmes, D.; Charleux, B. *Prog. Polym. Sci.* **2013**, *38*, 63–235.
[12] Moad, G.; Rizzardo, E.; Thang, S. H. *Aust. J. Chem.* **2012**, *65*, 985–1076.
[13] Moad, G. *Polym. Int.* **2015**, *64*, 15–24.
[14] Matyjaszweski, K. *J. Macromol. Sci.; Part A Pure Appl. Chem.* **1997**, *34*, 1785–1801.
[15] Amin, A.; Ayoub, M. H.; Abd El-Ghaffar, M.; Rieger, B. *J. Macromol. Sci.; Part A Pure Appl. Chem.* **2005**, *42*, 1329–1338.
[16] Feng, H.; Dan, Y. *J. Macromol. Sci.; Part A Pure Appl. Chem.* **2012**, *49*, 178–183.
[17] Wang, G.; Wu, H. *Polym. Bull.* **2011**, *67*, 1809–1821.
[18] Marcasuzaa, P.; Reynaud, S.; Grassl, B.; Preud'Homme, H.; Desbrières, J.; Trchovà, M.; Donard, O. F. X *Polymer* **2011**, *7*, 33–39.
[19] Hou, C.; Guo, Z.; Liu, J.; Ying, L.; Geng, D. *J. Appl. Polym. Sci.* **2007**, *104*, 1382–1385.
[20] Delfosse, S.; Borguet, Y.; Delaude, L.; Demonceau, A. *Macromol. Rapid. Communications* **2007**, *28*, 492–503.
[21] Li, N.; Lu, J.; Xu, Q.; Xia, X.; Wang, L. *Eur. Polym. J.* **2007**, *43*, 4486–4492.
[22] Li, J.; Zhu, X.; Zhu, J.; Cheng, Z. *Radiat. Phys. Chem.* **2007**, *76*, 23–26.
[23] Nguyen, C. T.; Nghiem, Q. D.; Kim, D.; Chang, J. S.; Hwang, Y. K. *Polymer* **2009**, *50*, 5037–5041.
[24] Roy, D.; Ullah, A.; Sumerlin, B. S. *Macromolecules* **2009**, *42*, 7701–7708.
[25] Özdemir, Z.; Topuzoğullari, M.; İşoğlu, I. A.; Dinçer, S. *Polym. Bull.* **2013**, *70*, 2857–2872.
[26] Rigolini, J.; Grassl, B.; Reynaud, S.; Billon, L. *J. Polym. Sci. Part A, Polym. Chem.* **2010**, *48*, 5775–5782.
[27] Rigolini, J.; Grassl, B.; Billon, L.; Reynaud, S.; Donard, O. F. X. *J. Polym. Sci. Part A: Polym. Chem.* **2009**, *47*, 6919–6931.
[28] Zhang, H.; Schubert, U. S. *Macromol. Rapid Communication* **2004**, *25*, 1225–1230.
[29] Sugihara, Y.; Semsarilar, M.; Perrier, S.; Zetterlund, P. B. *Polym. Chem.* **2012**, *3*, 2081–2086.
[30] Kwak, Y.; Mathers, R. T.; Matyjaszewski, K. *Macromol. Rapid Commun.* **2012**, *33*, 80–86.
[31] Herrero, M. A.; Kremsner, J. M.; Kappe, O. C. *J. Org. Chem.* **2008**, *73*, 36–47.
[32] Kappe, C. O. *Chem. Soc. Rev.* **2013**, *42*, 4977–4990.
[33] Aldana-García, M. A.; Palacios, J.; Vivaldo-Lima, E. *J. Macromol. Sci.; Part A Pure Appl. Chem.* **2005**, *42*, 1207–1225.
[34] Jaramillo-Soto, G.; Ramírez-Cupido, M.; Tenorio-López, J. A.; Vivaldo-Lima, E.; Penlidis, A. *Chem. Eng. Technol.* **2010**, *33*, 1888–1892.
[35] Hernandez-Meza, J. J.; Jaramillo-Soto, G.; Garcia-Moran, P. R.; Palacios-Alquisira, J.; Vivaldo-Lima, E. *Macromol. React. Eng.* **2009**, *3*, 101–107.
[36] López-Domínguez, P.; Vivaldo-Lima, E. *Macromol. React. Eng.* **2013**, *7*, 463–476.
[37] Hernandez-Ortiz, J. C.; Jaramillo-Soto, G.; Palacios-Alquisira, J.; Vivaldo-Lima, E. *Macromol. React. Eng.* **2010**, *4*, 210–221.
[38] Zetterlund, P. E.; Perrier, S. *Macromolecules* **2011**, *44*, 1340–1346.
[39] Roy, D.; Brent, S. S. *Polymer* **2011**, *52*, 3038–3045.
[40] Olvera-Mancilla, J.; López-Morales, S.; Palacios-Alquisira, J.; Morales-Morales, D.; Lagadec, R. L.; Alexandrova, L. *Polymer* **2014**, *55*, 1656–1665.
[41] Fernandez, S.; Pfeffer, M.; Ritleng, V.; Sirlin, C. *Organometallics* **1999**, *18*, 2390–2394.
[42] Ryabov, A. D.; Le Lagadec, R.; Estevez, H.; Alexandrova, L.; Fisher, A.; Pfeffer, M. *Inorg. Chem.* **2005**, *44*, 1626–1634.
[43] Wulkow, M. *Macromol. React. Eng.* **2008**, *2*, 461–494.
[44] Boutevin, B. J. *Polym. Sci.* **2000**, *38*, 3235–3243.
[45] Costa C, C.; Alberton, A. L.; Santos, A. F.; Fortuny, M.; Araújo, P. H. H.; Sayer, C.; Pinto, J. C. *Macromol. React. Eng.* **2015**, *9*, 366–373.
[46] Vivaldo-Lima, E.; Hamielec, A. E.; Wood, P. E. *Polym. React. Eng.* **1994**, *2* (1&2), 17–85.
[47] Achilias, D. J. *Appl. Polym. Sci.* **2010**, *116*, 1842–1856.
[48] Xia, J.; Paik, H.; Matyjasewski, K. *Macromolecules* **1999**, *32*, 8310–8314.
[49] Beuermann, S.; Buback, M. *Prog. Polym. Sci.* **2002**, *27*, 191–254.
[40] Li, H.; Zhang, Y. M.; Liu, Y. G. *J. Appl. Polym. Sci.* **2006**, *101*, 1089–1094.
[51] Mark, J. E. *Polymer Data Handbook*; Oxford University Press: New York, **1999**.